Competition between weak OH··· and CH··O hydrogen bonds: THz spectroscopy of the C2H2—H2O and C2H4—H2O complexes

Andersen, Jonas; Heimdal, Jimmy; Nelander, B.; Larsen, René Wugt

Published in:
Journal of Chemical Physics

Link to article, DOI:
10.1063/1.4983293

Publication date:
2017

Document Version
Peer reviewed version

Competition Between Weak OH··π and CH··O Hydrogen Bonds: THz Spectroscopy of the C_2H_2–H_2O and C_2H_4–H_2O Complexes

[a]J. Andersen, [a,b]J. Heimdal, [b]B. Nelander and [a]R. Wugt Larsen*

[a]*Department of Chemistry, Technical University of Denmark, Kemitorvet 206, 2800 Kgs. Lyngby, Denmark*

[b]*MAX-IV Laboratory, Lund University, P. O. Box 118, 22100 Lund, Sweden*

April 27, 2017

THz absorption spectra have been recorded for the weakly bound molecular complexes of H_2O with C_2H_4 and C_2H_2 embedded in cryogenic neon matrices at 2.8 K. The observation and assignment of a large-amplitude acceptor OH librational mode of the C_2H_2–H_2O complex at 145.5 cm^{-1} confirms an intermolecular CH··O hydrogen-bonded configuration of C_{2v} symmetry with the H_2O subunit acting as the hydrogen bond acceptor. The observation and assignment of two large-amplitude donor OH librational modes of the C_2H_4–H_2O complex at 255.0 and 187.5 cm^{-1}, respectively, confirms an intermolecular OH··π hydrogen-bonded configuration with the H_2O subunit acting as the hydrogen bond donor to the π-cloud of C_2H_4. A (semi)-empirical value for the change of vibrational zero-point energy of 4.0–4.1 kJ·mol^{-1} is proposed and the combination with quantum chemical calculations at the CCSD(T)-F12b/aug-cc-pVQZ level provides a reliable estimate of 7.1±0.3 kJ·mol^{-1} for the dissociation energy D_0 of the C_2H_4–H_2O complex. In addition, tentative assignments for the two strongly infrared active OH librational modes of the ternary C_2H_4–HOH–C_2H_4 complex having H_2O as a doubly OH··π hydrogen bond donor are proposed at 213.6 and 222.3 cm^{-1}. The present findings demonstrate that the relative stability of the weak hydrogen bond motifs are not entirely rooted in differences of electronic energy but also to a large extent by differences in the vibrational zero-point energy contributions arising from the class of large-amplitude intermolecular modes.

*Corresponding Author: rewl@kemi.dtu.dk

This manuscript was accepted by J. Chem. Phys. Click here to see the version of record.

1. Introduction

The class of non-covalent intermolecular interactions defined as hydrogen bonding is a concept of enormous importance for a vast number of physico-chemical phenomena within diverse scientific disciplines e.g. the thermodynamic phase behavior of fluid mixtures, the mechanical properties of functional polymers and the complex molecular organization of biological systems of relevance to the energy, material and life sciences, respectively. In simple terms the hydrogen bond has historically been defined as an interaction X–H··A wherein a hydrogen atom forms a "bond" between the two structural moieties X and A, of which one or even both moieties have a moderate to low electronegativity. Hydrogen bonding is now understood as a more complex phenomenon with dissociation energies spanning two order of magnitudes in the range from about 1 to 80 kJ·mol^{-1}.

The nature of a weak hydrogen bond is typically dominated by electrostatic and dispersion contributions, making a clear-cut distinction between a weak hydrogen bond and a strict "van der Waals interaction" rather challenging. The characterizing preference for linearity of hydrogen bonds becomes less pronounced as the relative electrostatic contributions become smaller. This varying directional behavior of weak hydrogen bonds has been demonstrated from comprehensive statistical crystallographic database surveys of weak C–H··O hydrogen bond interactions in crystalline samples, where the hydrogen bond donor strength of C–H groups depends on the hybridization of the involved C atoms in the order C(sp)–H > C(sp^2)–H > C(sp^3)–H. These kinds of crystallographic structural surveys may be blurred by crystal-field effects but statistical analyses of larger structural data sets have pointed to a significantly more directional behavior of C(sp)–H··O hydrogen bond motifs and even C(sp^3)–H··O hydrogen bond motifs relative to the isotropic non-linear contact geometries of strict van der Waals interactions.[1] The stabilization of hydrogen bonds between hydroxylic compounds and the π-electron clouds of olefins and aromatic compounds is another type of non-covalent interaction with more directional character than strict van der Waals interactions denoted weak OH··π hydrogen bonds.

The interaction energies of hydrogen bonding motifs revealed in crystalline samples cannot be extracted directly and quantitative measures of non-covalent intermolecular forces are often predicted for smaller molecular model systems *in vacuo* by high-level computational chemistry within the "supermolecular" approach. These hydrogen-bonded "supermolecules" or molecular complexes can be isolated in supersonic jet expansions, embedded in helium nanodroplets or cryogenic solid matrices and spectroscopically characterized to validate/falsify the intermolecular potential energy minima predicted by the hierarchy of quantum chemical calculations. These experimental approaches require both sufficient spectroscopic sensitivity and well-defined spectroscopic observables amenable to quantum chemical calculations. The intramolecular hydrogen bond donor X–H stretching vibrational mode of a hydrogen-bonded molecular complex is the most well-established mid-infrared spectroscopic indicator of hydrogen bonding. A strongly polar X–H bond usually gives rise to a pronounced spectral red-shift of the X–H stretching vibrational band origin in combination with a significant band broadening and gain in band intensity upon complexation relative to the "free" X–H stretching band.[1–3] A strong correlation

between the hydrogen bond strength and the donor X–H stretching red-shift has been established with relative spectral red-shifts in the order of ca. 5% for classically organic hydrogen-bonded systems.[2] The corresponding relative spectral red-shifts for weakly hydrogen-bonded systems is typically significantly smaller making it harder to distinguish clearly between weak hydrogen bonds and van der Waals interactions.

The two simplest "supermolecules" stabilized either by weak intermolecular C–H··O or OH··π hydrogen bond interactions, the mixed hydrogen-bonded molecular complexes of H_2O and C_2H_2 and C_2H_4, have both been intensively investigated by quantum chemical modeling but to a less degree by experimental work. The mixed C_2H_4–H_2O complex has previously been isolated in molecular beams and studied by both electric resonance microwave spectroscopy[4] and Fourier transform microwave spectroscopy[5] whereas the mid-infrared spectrum of this complex solely has been obtained in doped cryogenic matrices of argon.[6,7] The C_2H_2–H_2O complex has also previously been studied by molecular-beam electric resonance microwave spectroscopy[8] and the mid-infrared spectrum has been investigated by argon matrix isolation spectroscopy,[9] molecular-beam optothermal spectroscopy[10] and molecular-beam diode laser spectroscopy.[11] The hydrogen bond configurations of these hydrocarbon–water complexes were inferred *indirectly* by the sizes of the spectral shifts associated both with the strongly IR-active intramolecular donor X–H stretching modes in the mid-infrared spectral region. The spectral red-shift of the asymmetric C–H (and C–D) stretching mode of C_2H_2 has pointed at a weak intermolecular CH··O hydrogen-bonded configuration of the C_2H_2–H_2O complex with the C_2H_2 subunit acting as the hydrogen bond donor. In the case of the C_2H_4–H_2O complex the red-shifts associated with both the intramolecular symmetric and asymmetric O–H stretching modes of H_2O have indicated a weak intermolecular OH··π hydrogen-bonded configuration with the H_2O moiety as the hydrogen bond donor.

In recent works, it has been demonstrated how both the interaction strength, directionality and anharmonicity of OH··O hydrogen bonds in alcohol–H_2O complexes can be effectively probed *directly* via the class of large-amplitude intermolecular vibrational coordinates introduced upon complexation. These direct spectroscopic observables detected in the challenging far-infrared spectral region between 300 and 600 cm^{-1} have been shown to enable an accurate characterization of the conformational potential energy landscape spanned by the hydrogen-bonded subunits.[12–18] In the present work, we demonstrate how the class of large-amplitude hydrogen bond vibrational modes arising from the hindered rotational motion of the H_2O subunits in the THz region below 300 cm^{-1} provides *direct* excellent spectroscopic probes for the much weaker intermolecular CH··O and OH··π hydrogen bond motifs in these hydrocarbon–H_2O complexes. The infrared activity for large-amplitude librational modes of complexes between H_2O and non-polar hydrocarbons originates substantially from the dipole moment change associated with the hindered rotational motion of the H_2O subunits. Both the number of infrared active librational modes and their relative transition energies in the THz region depend directly on the hydrogen bond donor/acceptor role of the H_2O subunit.

This manuscript was accepted by J. Chem. Phys. Click here to see the version of record.

2. Experimental

Approximately 0.02 mol of neon gas (Air Liquide, 99.999%) was deposited onto a gold-plated oxygen-free high thermal conductivity copper mirror at 3.6 K in an immersion helium cryostat (IHC-3) customized for matrix isolation spectroscopy.[16,19] The neon gas was pre-cooled via a liquid nitrogen cooled (77 K) trap to achieve deposition flow rates in the range of 0.025 mol/h and the pre-cooled neon gas flow was subsequently doped with room temperature "freeze-pump-thaw" purified C_2H_4 (Sigma Aldrich, 99.9%), C_2H_2 (Sigma Aldrich, 99.9%), H_2O (Milli-Q) and isotopically substituted D_2O (Sigma Aldrich, 99.5% D) samples via separate inlet tubing systems with mixing ratios in the range of ≃0.05 to 0.5%. The use of resistive heating and feedback electronics maintained the mirror temperature at 2.8±0.1 K before and after the neon matrix deposition. Interchangeable CsI and polymethylpentene (TPX) windows were mounted on the vacuum shroud surrounding the cold cryostat head and IR and THz single-beam sample spectra were collected by a Bruker IFS 120 FTIR spectrometer. The IR single-beam spectra in the 600-4500 cm^{-1} region were all generated by a liquid nitrogen cooled narrow band HgCdTe detector combined with a Ge on KBr beam splitter and a globar radiation source. The THz single-beam spectra in the 30–650 cm^{-1} region were all generated by a liquid helium cooled Si-bolometer installed with three cold optical filters in combination with a 6 μm multilayer Mylar beam splitter and a globar radiation source. In most experiments the doped neon matrices were annealed up to 9 K and relaxed back to 3 K to facilitate the diffusion and thereby additional complex formation in the cryogenic matrix environments. Single-beam background spectra were all subsequently collected of the evacuated cryostat. A spectral resolution in the range from 0.1 to 1.0 cm^{-1} was selected depending on the observed band widths. In most cases the reported spectral bands could be reproduced with an error of 0.1 cm^{-1}.

3. Intermolecular Vibrational Assignments for the C_2H_2–H_2O Complex

Fig. 1 shows a series of THz absorption spectra (100–180 cm^{-1}) recorded at 2.8 K for cryogenic neon matrices doped with C_2H_2 (C_2H_2:Ne)=(1:500), H_2O or D_2O (H_2O:D_2O/Ne)=(1:1750) and a variety of C_2H_2/H_2O/D_2O mixtures (C_2H_2:H_2O:Ne)=(2:1:1000). A dominant spectral feature is observed at 79.5 cm^{-1} (not shown) for all the neon matrices doped with H_2O. This broad band including a high-wavenumber shoulder has previously been assigned to a rotational-translation-coupling (RTC) transition of monomeric H_2O embedded in solid neon[20] and thus provides an estimate of the H_2O concentration. In doped neon matrices with higher H_2O concentrations, several new distinct bands appear in the spectral region below 200 cm^{-1} which have previously been assigned to $(H_2O)_2$. The two strongest large-amplitude intermolecular fundamental vibrational transitions of $(H_2O)_2$ below 200 cm^{-1} in the THz region, the donor torsional mode and the acceptor wagging mode (a-axis libration), have previously been observed and assigned at 116.0 cm^{-1} and 122.2 cm^{-1} whereas the weaker fundamental transition associated with the in-plane acceptor c-axis librational mode has been assigned at 150.6 cm^{-1} in the neon matrix environment.[16,21–23]

THz spectra collected for neon matrices doped solely with C_2H_2 show no spectral evidence for any C_2H_2-containing cluster entities. The infrared active intramolecular vibrational fundamental transitions of C_2H_2 are all observed in the mid-infrared region (not shown) and observable number densities of weakly bound van der Waals clusters containing C_2H_2 are not expected in the employed concentration domain. Several previous microwave and infrared spectroscopic investigations have confirmed the existence of a T-shaped van der Waals interacting C_2H_2 dimer of C_{2v} symmetry.[24] Harmonic force field calculations at the MP2/aug-cc-pVTZ level for this T-shaped conformation of $(C_2H_2)_2$, however, predict no significantly infrared active large-amplitude vibrational transitions in the studied THz region supporting the present experimental findings.

The simultaneous use of both C_2H_2 and H_2O as dopants in neon matrices allows the identification of one new distinct and reproducible band located at 145.5 cm^{-1} (Fig. 1, the blue trace). The intensity of this band increases linearly both with added H_2O and added C_2H_2 suggesting the assignment to a 1:1 complex of H_2O and C_2H_2. In order to support this vibrational assignment a series of THz spectra have been collected for neon matrices doped simultaneously with $C_2H_2/D_2O/H_2O$ samples with a varying relative D_2O content. Fig. 1 shows the THz spectra collected for neon matrices doped with C_2H_2 and an almost pure D_2O sample (the red trace) and a mixed D_2O:H_2O sample with a mixing ratio of ca. 3:1 (the green trace). This series of THz spectra clearly reproduces two new distinct bands at 127.8 cm^{-1} and 119.1 cm^{-1} red-shifted by 17.7 cm^{-1} and 26.4 cm^{-1}, respectively, relative to the 145.5 cm^{-1} band. None of these new bands appear in the absence of C_2H_2 and the mostly red-shifted band observed at 119.1 cm^{-1} can easily be assigned to the 1:1 complex of C_2H_2 and D_2O by this concentration series alone whereas the band observed 127.8 cm^{-1} must be assigned to a 1:1 complex of C_2H_2 and HDO. The latter assignment is unambigiously confirmed by the quantum chemical vibrational spectral shift predictions described in section 6 and given in the supplementary material.
The observation of one single intermolecular large-amplitude vibrational mode in the THz region below 200 cm^{-1} for the 1:1 complex indicates *directly* a weak intermolecular C–H··O hydrogen bond configuration with H_2O as the hydrogen bond acceptor. A strongly infrared active transition associated with an in-plane acceptor *c*-axis librational mode is expected below 200 cm^{-1} for this conformation. The observed band origin of 145.5 cm^{-1} seems reasonable since the corresponding in-plane acceptor *c*-axis librational mode of the stronger $(H_2O)_2$ complex has been observed at 150.6 cm^{-1} in neon matrices.[16] A second strongly infrared active transition associated with the out-of-plane acceptor *a*-axis librational mode of this conformation is predicted below 50 cm^{-1} by exploratory quantum chemical calculations described in more details in section 6. This acceptor *a*-axis librational mode is thus shifted significantly relative to the observation for the $(H_2O)_2$ complex. A weak intermolecular OH··π hydrogen-bonded configuration with H_2O as the hydrogen bond donor, on the other hand, would give rise to two infrared active transitions associated with large-amplitude donor OH librational modes in the region above 150 cm^{-1} (section 6).

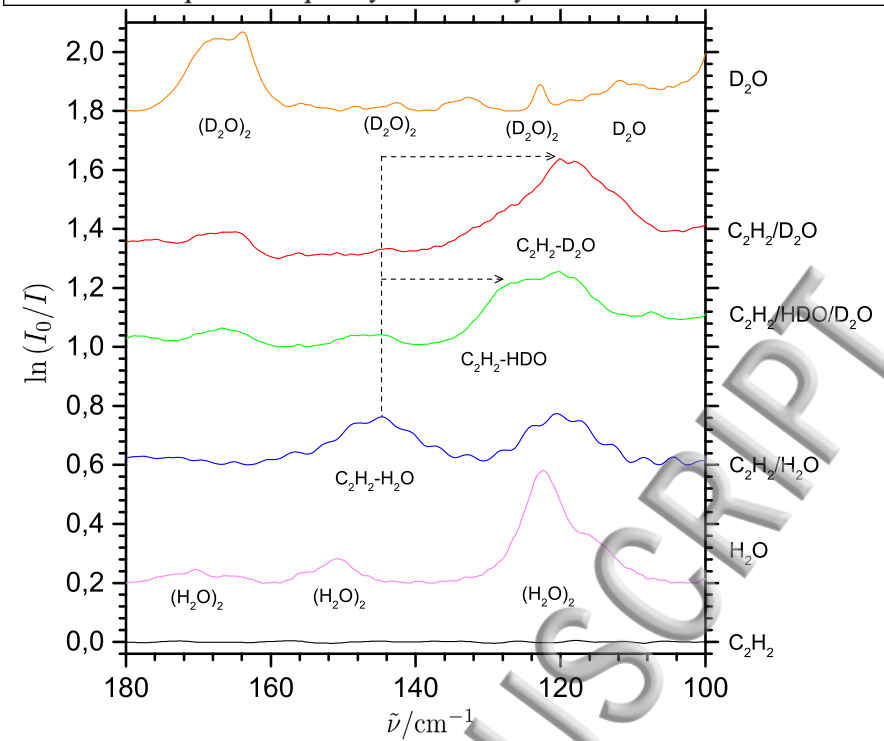

Figure 1: The observed THz absorption spectra (100–200 cm^{-1}) of C_2H_2, H_2O and several $C_2H_2/H_2O/D_2O$ mixtures embedded in neon matrices at 2.8 K. The proposed vibrational assignments and isotopic spectral shifts of the large-amplitude acceptor *c*-axis librational band of the C_2H_2-H_2O complex are indicated.

4. Intermolecular Vibrational Assignments for the C_2H_4–H_2O Complex

Fig. 2 shows a series of THz absorption spectra (100–300 cm^{-1}) recorded for cryogenic neon matrices at 2.8 K doped with C_2H_4 (C_2H_4:Ne)=(1:1100), H_2O or D_2O (H_2O:D_2O/Ne)=(1:1750) and a variety of $C_2H_4/H_2O/D_2O$ mixtures (C_2H_4:H_2O:Ne)=(2:1:1000–3000). In this extended spectral region another distinct band at 227 cm^{-1} has previously been assigned to $(H_2O)_2$[25] and the band observed at 280 cm^{-1} has previously been assigned to $(H_2O)_3$.[26] THz absorption spectra of neon matrices doped solely with C_2H_4 (not shown) do not reveal any absorption bands. The intramolecular vibrational fundamental bands of monomeric C_2H_4 are all observed in the mid-infrared region (not shown) and observable number densities of weakly bound van der Waals complexes of C_2H_4 are not expected for the employed Ne:C_2H_4 mixing ratios. A recent quantum chemical modeling investigation of the van der Waals homodimer $(C_2H_4)_2$[27] reported a CCSD(T) dissociation energy at the equilibrium structure in the basis set limit of just 6.32 $kJ{\cdot}mol^{-1}$. This theoretical work did not predict any significantly infrared active large-amplitude intermolecular transitions in the studied THz region and thus supports our experimental findings.

In neon matrices doped simultaneously with H_2O and C_2H_4 one new distinct band appears at 187.5 cm^{-1} (Fig. 2). The intensity of this band increases linearly both with the concentration

This manuscript was accepted by J. Chem. Phys. Click here to see the version of record.

of added H_2O and added C_2H_4 and can thus unambiguously be assigned to a 1:1 complex of H_2O and C_2H_4. At higher concentrations of H_2O two additional spectral features appear; a very weak but still distinct band at 255.0 cm^{-1} together with two stronger overlapping bands at 213.6 cm^{-1} and 222.3 cm^{-1} (Fig. 2, the red trace). The intensity of the 255.0 cm^{-1} band as for the 187.5 cm^{-1} band increases linearly both with added H_2O and added C_2H_4 which supports an assignment to the 1:1 complex of H_2O and C_2H_4. The intensities of the overlapping bands observed at 213.6 cm^{-1} and 222.3 cm^{-1}, however, both scale more rapidly with the concentration of C_2H_4 pointing at a ternary $H_2O(C_2H_4)_2$ complex with H_2O as a doubly hydrogen bond donor. These tentative assignments for a ternary $H_2O(C_2H_4)_2$ complex shall be discussed further in the section 6 concerning exploratory quantum chemical calculations.

The observation of two THz bands associated with intermolecular large-amplitude vibrational transitions above 150 cm^{-1} for the 1:1 complex of H_2O and C_2H_4 indicates a weak intermolecular OH··π hydrogen bond configuration with H_2O as the hydrogen bond donor. In this global potential energy minimum two observable donor OH librational modes are expected; a highly localized out-of-plane OH librational mode and an in-plane OH librational mode resembling a hindered overall c-axis rotation of the water subunit (see section 6). In order to confirm these assignments further, a series of THz spectra have been collected for neon matrices doped simultaneously with $C_2H_4/H_2O/D_2O$. The insert of Fig. 2 illustrates both the effect of the full and the partly isotopic H/D exchange on the H_2O moiety. The isotopic spectral shifts of the very weak band at 255.0 cm^{-1} are not observable as the weak H/D shifted bands are expected close to 200 cm^{-1} in the vicinity of the stronger 187.5 cm^{-1} band. However, significant isotopic spectral red-shifts are observed for the 187.5 cm^{-1} band. Two new distinct bands are observed at 168.7 cm^{-1} and 149.0 cm^{-1} with a relative intensity depending on the D_2O:H_2O mixing ratio. The relative intensity of the mostly red-shifted band at 149.0 cm^{-1} is significantly higher for larger D_2O:H_2O mixing ratios pointing at an assignment to the 1:1 complex of C_2H_4 and D_2O. It should be noted here that the in-plane acceptor c-axis libration fundamental transition assigned at 150.6 cm^{-1} for $(H_2O)_2$ is shifted to 118.0 cm^{-1} for $(D_2O)_2$ and does not contribute to the absorption observed at 149.0 cm^{-1} in the insert of Fig. 2 (the black trace). The less shifted band at at 168.7 cm^{-1} appears whenever the neon matrices are doped with significant amounts of D_2O with a maximum relative intensity for matrices with equal amounts of embedded D_2O and H_2O. These findings clearly support an assignment to the 1:1 complex of HDO with C_2H_4 having a weak intermolecular OD··π deuterium bond to the π-cloud of C_2H_4 as supported by the harmonic force field predictions described in section 6 and provided in the supplementary material. In addition, we note that in the harmonic approximation the librational band origins are proportional to the square root of the corresponding rotational constants for the isolated subunit. The inspection of the values for the rotational constants C_0 of H_2O, HDO and D_2O,[28] predicts the band origins of 161 and 140 cm^{-1} for the c-axis librational modes of the C_2H_4–HDO and C_2H_4–D_2O complexes, respectively. This simple harmonic picture also supports qualitatively the experimental isotopic spectral shifts.

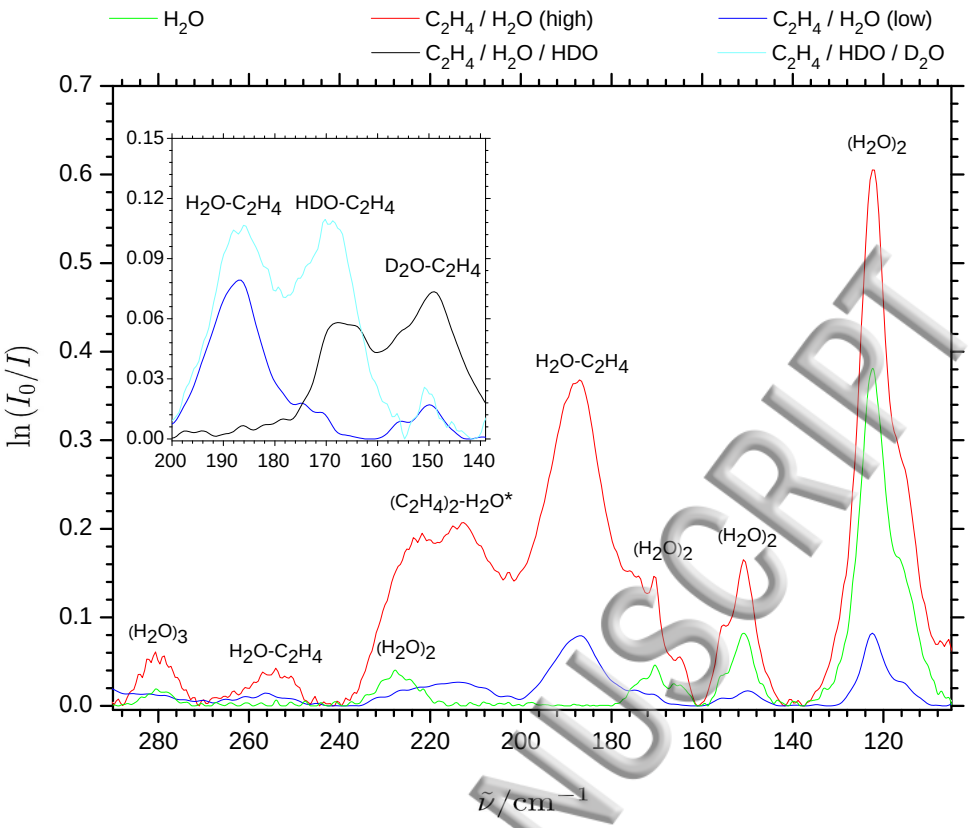

Figure 2: The observed THz absorption spectra (100–300 cm^{-1}) of ethylene, regular and isotopically enriched water and several isotopic ethylene-water mixtures embedded in neon matrices at 2.8 K. The proposed vibrational assignments of the two large-amplitude donor OH librational bands of the ethylene-water complex are indicated and the isotopic spectral shifts are shown in the insert. The tentative assignments for the ternary $H_2O(C_2H_4)_2$ complex are marked with asterisks.

5. Exploratory Quantum Chemical Calculations

The quantum chemical software packages Gaussian09 (Rev. D.01)[29] and MOLPRO (ver. 2012.1)[30,31] have been employed for *ab initio* electronic structure calculations. The potential energy minima geometries of the monomers and the mixed hydrogen-bonded hydrocarbon-water complexes have all been optimized using the second-order Möller-Plesset MP2 method[32,33] combined with Dunning's family of augmented correlation-consistent triple-zeta (aug-cc-pVTZ) and quadruple-zeta (aug-cc-pVQZ) basis sets.[34] The single-point electronic energies for these optimized minima structures were subsequently furthermore computed employing both the coupled-cluster approach with single and double excitations and perturbative treatment of triple excitations CCSD(T)[35] and the explicitly-correlated CCSD(T)-F12b methodology[36] implemented in MOLPRO combined with the same basis sets to optimize the description of electron correlation. The effects of the basis set superposition errors[37] have been accounted for by the implemented counterpoise methods.[38] The calculated absolute electronic energies from the MP2, CCSD(T) and CCSD(T)-F12b methods with the aug-cc-pVQZ basis set, the

This manuscript was accepted by J. Chem. Phys. Click here to see the version of record.

electronic complexation energies D_e, the predicted harmonic vibrational zero-point energy corrections employing the MP2/aug-cc-pVQZ level and the resulting dissociation energies D_0 are provided in the electronic supplementary information.

6. Results and Discussion

6.1 The Hydrogen-Bonded 1:1 Complex of Acetylene and Water

The quantum chemical calculations at the CCSD(T)-F12b/aug-cc-pVQZ level agree with previous theoretical work[39,40] and the previous and present experimental findings pointing at a weak and strictly linear intermolecular CH··O hydrogen-bonded configuration of C_{2v} symmetry with the C_2H_2 subunit acting as the hydrogen bond donor (denoted conformer I, D_e = 12.3 kJ·mol^{-1}). In the microwave work by Peterson and Klemperer, they considered the isotopic shift of the dipole moment for the C_2H_2–H_2O complex to investigate whether the system is planar or has a pyramidal structure.[8] The observed increase of the dipole moment upon deuteration of the H_2O subunit helped them to conclude, that a hypothetical pyramidal structure must have a barrier so low that even the the ground state has an energy above the barrier. In the theoretical work by Xantheas *et al.*,[39] it was found that quantum chemical methodologies tend to predict a pyramidal potential energy minimum but that the barrier decreases with the basis set size and completely vanishes when vibrational zero-point energy contributions are incorporated. We note that for the $(H_2O)_2$ complex, the angle between the *b*-axis of the acceptor subunit and the intermolecular hydrogen bond is approximately 60 degrees possible due to electrostatic repulsion between the acceptor hydrogen atoms and the free hydrogen atom of the donor subunit. In the C_2H_2–H_2O complex the *b*-axis of the H_2O subunit coincides with the hydrogen bond and this may explain the much higher transition energy of the out-of-plane acceptor *b*-axis librational fundamental in the $(H_2O)_2$ complex compared to the C_2H_2–H_2O complex.

In addition to the global potential energy minimum, a local potential energy minimum involves a weak intermolecular OH··π hydrogen bond with the H_2O subunit as a hydrogen bond donor to the π-cloud of C_2H_2 (denoted conformer II, D_e = 10.95 kJ·mol^{-1}). Fig. 3 illustrates these two different CH··O and OH··π hydrogen-bonded conformations of the C_2H_2–H_2O complex and provides both the electronic dissociation energy D_e and the vibrational zero-point corrected dissociation energy D_0 for the two different conformations. The fundamental vibrational band origins and corresponding infrared band intensities predicted at the MP2/aug-cc-pVQZ level in the doubly harmonic approximation for both these conformations are given in Table 1. This table provides the predicted harmonic band origins for the perturbed intramolecular vibrational modes, the predicted harmonic vibrational spectral complexation shifts relative to the isolated monomers $\Delta\omega = \omega_{com}$–$\omega_{mon}$ and the predicted harmonic band origins for the large-amplitude intermolecular vibrational modes introduced upon complexation.

The CCSD(T)-F12b/aug-cc-pVQZ electronic energy difference of ca. 1.3 kJ·mol^{-1} between the CH··O and OH··π hydrogen bond motifs in the equilibrium configurations increases to 2.8

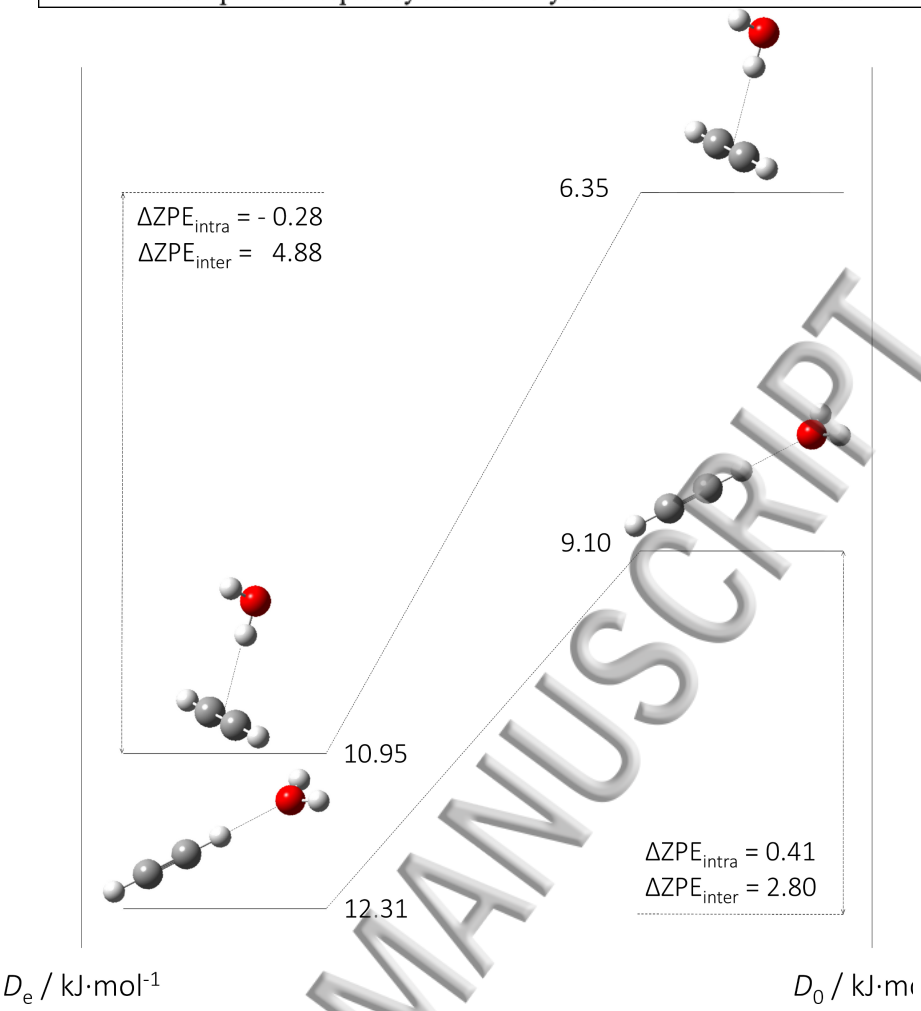

Figure 3: The predicted conformational potential energy landscape of the C_2H_2–H_2O complex showing both the electronic dissociation energies D_e at the CCSD(T)-F12b/aug-cc-pVQZ level, the change of vibrational zero-point energy associated with perturbed intramolecular modes ΔZPE_{intra} and large-amplitude intermolecular modes ΔZPE_{inter} at the MP2/aug-cc-pVQZ level and the resulting dissociation energies D_0 at 0 K.

kJ·mol^{-1} between the corresponding dissociation energies D_0 when the harmonic vibrational zero-point contributions are incorporated. The contribution from the spectral shifts of perturbed intramolecular vibrational transitions is dominated by spectral shifts of the hydrogen bond donor; spectral red-shifts for the intramolecular X–H stretching modes and spectral blue-shifts for the intramolecular bending modes. The net contributions to the conformational energy difference is very small for the class of intramolecular vibrational modes as illustrated in Table 1. In the global potential energy minimum, the two doubly degenerate vibrational modes associated with the symmetric and asymmetric CCH deformation modes of the isolated C_2H_2 subunit are no longer degenerate upon complexation with H_2O due to the broken cylindrical symmetry. Both the symmetric and asymmetric CCH deformation modes of the C_2H_2 subunit are split into two different in-plane and out-of-plane components which are blue-shifted relative to the monomeric C_2H_2 fundamentals. However, the complexation spectral shifts associated with the

Table 1: MP2/aug-cc-pVQZ predictions in the double harmonic approximation of the vibrational band origins (units of cm^{-1}) and corresponding infrared band strengths (units of $km \cdot mol^{-1}$, in parenthesis) for H_2O, C_2H_2 and the two most stable conformations of the C_2H_2–H_2O complex. The predicted harmonic complexation spectral shifts ($\Delta\omega = \omega_{com} - \omega_{mon}$) and observed (anharmonic) spectral shifts ($\Delta\nu_{obs} = \nu_{com,obs} - \nu_{mon,obs}$) of the intramolecular vibrational transitions together with harmonic band origins of the intermolecular large-amplitude vibrational transitions are given for both conformations

$\omega(H_2O)$	$\omega(C_2H_2)$	ω(Conformer I)	$\Delta\omega$	ω(Conformer II)	$\Delta\omega$	$\Delta\nu_{obs}$
		Intra-molecular		*Intra*-molecular		
3965.5 (78)		3962.2 (91)	–3.4	3938.4 (144)	–27.1	
1632.4 (73)		1633.7 (68)	1.3	1637.7 (56)	5.3	4.0[a]; 7.0[b]
3839.7 (6.1)		3838.0 (12)	–1.7	3801.6 (113)	–38.1	2.0[a]; –2.8[b]
	3530.2 (0.0)	3510.2 (0.1)	–20.1	3522.7 (0.1)	–7.5	
	1975.1 (0.0)	1965.9 (7.6)	–9.2	1970.8 (0.3)	–4.3	
	3442.6 (96)	3398.5 (249)	–44.1	3434.9 (111)	–7.7	–48.7[a]; –34.5[b]
	613.6 (0.0)	638.1 (8.7)	24.5	628.4 (1.2)	14.7	
		633.3 (7.8)	19.6	616.3 (0)	2.7	
	750.3 (198)	810.2 (78)	59.9	762.5 (98)	12.2	56.2[a]; 46.1[b]
		792.6 (75)	42.3	754.0 (86)	3.7	49.2[a]; 40.2[b]
		Inter-molecular		*Inter*-molecular		
		180.4(36)		375.0 (49)		
		115.2(1.4)		171.6 (71)		
		93.7(6.6)		116.3 (78)		
		53.5(28)		109.3 (2.1)		
		24.4(225)		42.9 (27)		

[a] Ref.[9]

[b] Present work

infrared inactive degenerate symmetric CCH deformation and the symmetric C–H stretching modes of monomeric C_2H_2 cannot easily be verified by direct absorption spectroscopy. The predicted harmonic spectral shifts for the most stable CH··O hydrogen bond motif (conformer I) are compared to the experimental spectral shifts when available both from the present neon matrix data and previous experimental work in Table 1. The sum of harmonically predicted spectral shifts associated with the intramolecular vibrational modes in general seems to agree qualitatively with the experimental results which is most likely due to counteracting diagonal and off-diagonal anharmonic contributions.[2] The spectral shifts of the perturbed intramolecular vibrational modes sum up to 68 cm^{-1} and –53 cm^{-1} for conformer I and conformer II, respectively, according to the harmonic MP2/aug-cc-pVQZ predictions giving contributions to the change of vibrational zero-point energy in the order of $\pm$(0.3–0.4) $kJ \cdot mol^{-1}$ as illustrated in Fig. 3. These contributions from the perturbed intramolecular vibrational motion as such

This manuscript was accepted by J. Chem. Phys. Click here to see the version of record.

constitute a minor portion of the total change of vibrational zero-point energy upon complexation.

The quantum chemical predictions clearly demonstrate that the relative stability of the two different hydrogen bond motifs are not entirely rooted in differences of electronic energy (1.3 kJ·mol^{-1}) but to a significant extent by different vibrational zero-point energy contributions from the five large-amplitude intermolecular fundamental modes. The minor stable OH··π hydrogen bond motif (conformer II), in particular, introduces two donor OH librational modes with harmonic band origins predicted at 375 and 172 cm^{-1}; a highly localized out-of-plane OH librational mode together with an in-plane OH librational mode resembling a hindered overall c-axis rotation of the water subunit as visualized in Fig. 4. The predicted harmonic vibrational zero-point energy contribution of 3.25 kJ·mol^{-1} associated with these two large-amplitude intermolecular OH librational modes alone extends the entire harmonic vibrational zero-point energy contribution from the five large-amplitude intermolecular modes for the most stable conformer I of 2.8 kJ·mol^{-1}. The total harmonic vibrational zero-point energy contribution from the class of large-amplitude intermolecular modes of conformer II is 4.9 kJ·mol^{-1} according to the MP2/aug-cc-pVQZ predictions as illustrated in Fig. 3.

The highest intermolecular vibrational fundamental transition energy for conformer I is predicted to be just 180 cm^{-1} in the harmonic approximation which is associated with the large-amplitude H_2O in-plane c-axis libration as illustrated in Fig. 4. The harmonic prediction for this infrared active in-plane c-axis libration significantly overestimates the experimental anharmonic band origin observed at 145.5 cm^{-1} in the doped neon matrices. The observation and assignment of one single intermolecular vibrational band for the C_2H_2–H_2O complex makes it hard to quantify the total anharmonic vibrational zero-point energy contribution from this class of large-amplitude intermolecular vibrational modes. However, anharmonicity contributions in the same order of 15-20% for large-amplitude intermolecular vibrational modes have been observed for a variety of more strongly OH··O hydrogen-bonded molecular complexes.[14,17,18] The predicted (harmonic) value of the dissociation energy D_0 of 11.3 kJ·mol^{-1} for the most stable conformation of the 1:1 C_2H_2–H_2O complex should thus be regarded as a lower limit relative to the true value including anharmonicity corrections.

6.2 The Hydrogen-Bonded 1:1 Complex of Ethylene and Water

The present quantum chemical calculations support the previous[4–7] and present experimental findings that the global potential energy minimum of the 1:1 complex of C_2H_4 and H_2O involves a weak intermolecular OH··π hydrogen bond motif with the H_2O subunit acting as the hydrogen bond donor. Extensive computational efforts to find another local potential energy conformation involving a weak intermolecular CH··O hydrogen bond motif with the C_2H_4 subunit as the hydrogen bond donor were not successful. The CCSD(T)-F12b/aug-cc-pVQZ electronic dissociation energy computed at the equilibrium configuration D_e is 10.9 kJ·mol^{-1} for the most stable OH··π hydrogen bond motif of the C_2H_4–H_2O complex (see supplemen-

tary material). These calculations indicate that the electronic dissociation energy D_e is almost identical for the two OH··π hydrogen bond motifs in the C_2H_2–H_2O (10.95 kJ·mol^{-1}) and C_2H_4–H_2O (10.90 kJ·mol^{-1}) complexes and thereby almost independent of the hybridization of the involved C atoms. This electronic dissociation energy D_e is, however, 1.4 kJ·mol^{-1} smaller than the corresponding D_e-value for the CH··O hydrogen bond motif of the C_2H_2–H_2O complex.

The electronic dissociation energy of 10.90 kJ·mol^{-1} for the equilibrium configuration for the C_2H_4–H_2O complex translates into a D_0-value of 5.90 kJ·mol^{-1} when predicted harmonic vibrational zero-point energy contributions are incorporated. The MP2/aug-cc-pVQZ predictions for the C_2H_4–H_2O complex in the doubly harmonic approximation are provided in Table 2 which lists the harmonic band origins for the perturbed intramolecular vibrational modes, harmonic vibrational complexation shifts relative to the isolated monomers $\Delta\omega = \omega_{com}$–$\omega_{mon}$ and harmonic band origins for the large-amplitude intermolecular vibrational modes introduced by complexation. The most pronounced spectral red-shifts of the intramolecular symmetric and asymmetric O–H stretching modes of the H_2O subunit and the smaller spectral blue-shifts of the two CH_2 wagging modes of the C_2H_4 subunit. Together these spectral shifts contribute –0.32 kJ·mol^{-1} to the change of vibrational zero-point energy. This value is adjusted to –0.17 kJ·mol^{-1} when the remaining intramolecular harmonic spectral shifts are incorporated. This contribution from the perturbed intramolecular vibrational motion thus constitute an even smaller portion of the total change of vibrational zero-point energy than observed for the C_2H_2–H_2O complex.

The OH··π hydrogen bond configuration gives rise to two large-amplitude intermolecular OH librational modes; a highly localized out-of-plane OH librational mode and an in-plane OH librational mode resembling a hindered overall c-axis rotation of the H_2O subunit which are illustrated in Fig. 4. The harmonic band origins for these donor OH librational modes are predicted at 345 and 240 cm^{-1}, respectively, and these two modes alone constitute approximately 2/3 (3.5 kJ·mol^{-1}) of the total change of vibrational zero-point energy ΔZPE (5.3 kJ·mol^{-1}) introduced by the hydrogen bond formation from the six large-amplitude intermolecular modes. The fact that 2/3 of the value is verified experimentally from the present observations enables a reliable semi-empirical estimate of ΔZPE. The largest error bar stems from the anharmonic character of the four remaining large-amplitude vibrational transitions which are all predicted below 110 cm^{-1} in the harmonic approximation (Table 2). The proposed experimental assignments at 255.0 and 187.5 cm^{-1} for the two donor OH librational modes indicate substantial anharmonicity contributions in the order of 20-25% for this class of intermolecular vibrational modes. The total anharmonic contributions thus sum up to 60–75 cm^{-1} for the four remaining large-amplitude intermolecular modes assuming similar 20–25% relative anharmonicity for these modes. The resulting semi-empirical value of ΔZPE based on the observed fundamental band origins and anharmonic band origin predictions of the four non-observed fundamentals then sums up to 3.8–3.9 kJ·mol^{-1} instead of the full MP2/aug–cc-pVQZ prediction of 5.0 kJ·mole^{-1} in the harmonic approximation. The combined electronic dissociation energy of 10.90 kJ·mol^{-1} for the equilibrium configuration and this semi-empirical value of ΔZPE translates into a D_0-

This manuscript was accepted by J. Chem. Phys. Click here to see the version of record.

Table 2: MP2/aug-cc-pVQZ predictions in the double harmonic approximation of the vibrational band origins (units of cm^{-1}) and corresponding infrared band strengths (units of $km \cdot mol^{-1}$, in parenthesis) for H_2O, C_2H_4 and the most stable OH··π conformation of the C_2H_4–H_2O complex. The predicted harmonic complexation spectral shifts ($\Delta\omega = \omega_{com}$–$\omega_{mon}$) and observed (anharmonic) spectral shifts ($\Delta\nu_{obs} = \nu_{com,obs}$–$\nu_{mon,obs}$) of the intramolecular vibrational transitions together with harmonic band origins of the intermolecular large-amplitude vibrational transitions are given.

$\omega(H_2O)$	$\omega(C_2H_4)$	ω(Complex)	$\Delta\omega$	$\Delta\nu_{obs}$
		Intra-molecular		
3965.5 (78)		3937.2 (150)	–28.3	–16.8[a]; –22.8[b]
1632.4 (73)		1637.2 (40)	4.8	5.6[a]
3839.7 (6.1)		3791.2 (126)	–48.5	–37.2[b]
	3193.4 (0.0)	3191.4 (0.2)	–2.0	
	1680.3 (0.0)	1674.7 (0.3)	–5.6	
	1381.3 (0.0)	1380.8 (0.0)	–0.5	
	1072.9 (0.0)	1078.0 (0.0)	5.1	
	3267.5 (0.0)	3268.2 (0.2)	0.7	
	1249.4 (0.0)	1250.7 (0.2)	1.3	
	979.9 (91)	993.5 (101)	13.5	12.2[a]; 7.8[b]
	963.9 (0.0)	974.0 (0.0)	10.1	
	3293.8 (12)	3293.9 (6.2)	0.1	
	823.3 (0.0)	824.2 (0.2)	0.9	
	3177.2 (9.2)	3176.6 (4.6)	–0.6	
	1481.4 (9.2)	1482.7 (10.2)	1.3	
		Inter-molecular		
		345.1 (37)		
		239.6 (84)		
		109.0 (1)		
		79.3 (37)		
		67.4 (17)		
		42.7 (82)		

[a] Ref.[6]

[b] Present work

value of ca. 7.00-7.10 $kJ \cdot mol^{-1}$. If residual anharmonicity contributions in the order of ±25 cm^{-1} are taken into account together with potential matrix spectral shifts in the ±25 cm^{-1} range, we arrive at a best estimate of 7.1±0.3 $kJ \cdot mol^{-1}$ for the dissociation energy at 0 K.

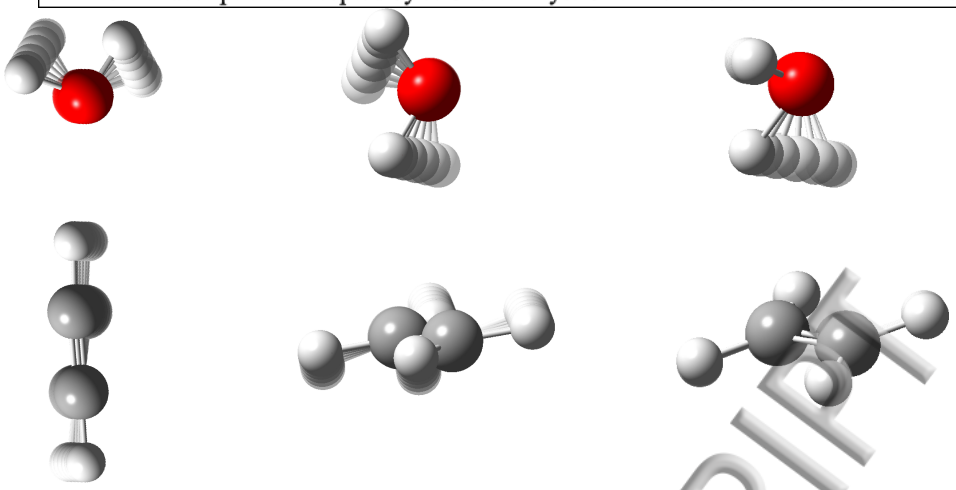

Figure 4: Animations of the assigned intermolecular large-amplitude vibrational normal modes: Left) The in-plane acceptor rocking (c-axis libration) mode of the C_2H_2–H_2O complex. Center) The low-frequency in-plane donor OH librational (c-axis libration) mode of the C_2H_4–H_2O complex. Right) The high-frequency out-of-plane donor OH librational mode of the C_2H_4–H_2O complex.

6.3 The Hydrogen-Bonded Ternary Complexes of Ethylene and Water

In all matrix isolation experiments where neon matrices are doped simultaneously with C_2H_4 and H_2O a broad absorption feature is observed in the 205–240 cm^{-1} spectral region (Fig. 2). In the high concentration regime where the weaker high-frequency donor OH librational band of the 1:1 C_2H_4–H_2O complex at 255.0 cm^{-1} is clearly observable this broad spectral feature appears as two distinct bands of almost identical intensity centered at 213.6 and 222.3 cm^{-1}. The appearance of these two bands at the high dopant concentrations point at potential assignments to ternary complexes of C_2H_4 and H_2O. In most experiments an excess of C_2H_4 relative to H_2O have been employed to prevent formation of $(H_2O)_2$ and this at first sight then suggest the assignments to the ternary $H_2O(C_2H_4)_2$ complex.

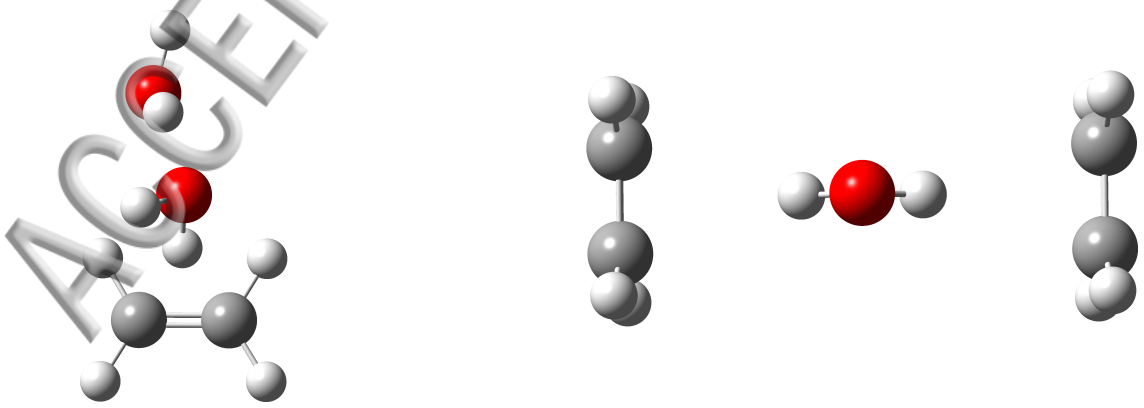

Figure 5: The potential energy minima geometries of the two different ternary $(H_2O)_2C_2H_4$ (left) and $H_2O(C_2H_4)_2$ (right) complexes optimized at the MP2/aug-cc-pVTZ level of theory.

The quantum chemical geometry optimizations at the MP2/aug-cc-pVTZ level predict potential energy minima for two ternary complexes $H_2O(C_2H_4)_2$ and $(H_2O)_2C_2H_4$ as shown in Fig. 5. In the first ternary complex $(H_2O)_2C_2H_4$ the predicted potential energy minimum is based on a $(H_2O)_2$ complex where the hydrogen bond acceptor subunit forms a weak intermolecular OH$\cdot\cdot\pi$ hydrogen bond to the C=C bond of the C_2H_4 subunit. In the second ternary $H_2O(C_2H_4)_2$ complex the H_2O molecule acts as a doubly OH$\cdot\cdot\pi$ hydrogen bond donor to two separate C_2H_4 molecules. Table 3 lists the corresponding MP2/aug-cc-pVTZ predictions of the harmonic band origins for the classes of large-amplitude intermolecular vibrations for both ternary complexes of C_2H_4 and H_2O. These harmonic predictions support a tentative assignment of the two observed bands to the ternary $H_2O(C_2H_4)_2$ complex containing two C_2H_4 molecules as two strongly IR-active OH librational modes are predicted at 316 and 321 cm^{-1} for this doubly OH$\cdot\cdot\pi$ hydrogen bonded structure. The two strongly IR-active intermolecular modes can both be described as librational modes; the low-frequency mode describes the hindered rotation of the H_2O molecule out of the mirror plane spanned by the two intermolecular OH$\cdot\cdot\pi$ hydrogen bonds whereas the high-frequency mode describes the hindered rotation of the H_2O molecule in this mirror plane as depicted in Fig. 6. If we assume anharmonic contributions in the same 20-25%-range as observed for the 1:1 complexes the scaled harmonic predictions for the ternary $H_2O(C_2H_4)_2$ complex are en fairly good agreement with the observations.

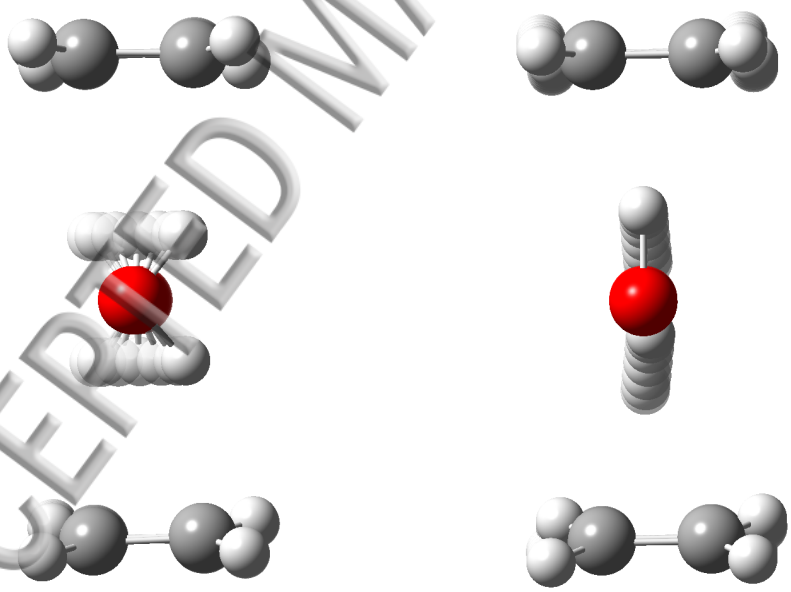

Figure 6: Animations of the two IR-active librational modes of the ternary $H_2O(C_2H_4)_2$ complex. Left) The hindered rotation of the water molecule out of the mirror plane spanned by the two intermolecular OH$\cdot\cdot\pi$ hydrogen bonds. Right) The hindered rotation of the water molecule in the mirror plane spanned by the two intermolecular OH$\cdot\cdot\pi$ hydrogen bonds.

Table 3: Harmonic MP2/aug-cc-pVTZ predictions for the classes of intermolecular large-amplitude vibrational band origins (units of cm^{-1}) and corresponding infrared band strengths (units of $km \cdot mol^{-1}$, in parenthesis) for the potential energy minima of the ternary $H_2O(C_2H_4)_2$ and $(H_2O)_2C_2H_4$ complexes.

ω(C_2H_4–H_2O–C_2H_4)	ω(H_2O–H_2O–C_2H_4)
385.6 (0.0)	612.4 (91.3)
320.8 (111.4)	501.2 (55.3)
315.5 (87.0)	301.0 (161.8)
118.4 (0.0)	250.1 (78.9)
118.3 (0.2)	189.6 (17.7)
74.4 (0.0)	180.1 (0.7)
63.3 (0.0)	175.1 (74.2)
57.6 (7.2)	128.9 (96.1)
55.0 (12.8)	120.4 (2.5)
14.8 (0.3)	98.2 (3.8)
11.5 (1.2)	77.0 (9.3)
9.6 (0.0)	27.6 (3.1)

7. Conclusions

The absorption spectra in the sub-10 THz range have been collected for the weakly bound C_2H_2–H_2O and C_2H_4–H_2O complexes embedded in cryogenic neon matrices at 2.8 K and have provided the first observation and assignments of several characteristic large-amplitude intermolecular hydrogen bond vibrational modes. The assigned large-amplitude acceptor in-plane c-axis librational mode of the 1:1 C_2H_2–H_2O complex observed at 145.5 cm^{-1} confirms a strictly linear intermolecular CH··O hydrogen-bonded conformation with C_{2v} symmetry having the H_2O subunit as the hydrogen bond acceptor. This global potential energy minimum is supported by quantum chemical calculations at the CCSD(T)-F12b/aug-cc-pVQZ level. A lower limit for the dissociation energy D_0 at 0 K of 11.3 $kJ \cdot mol^{-1}$ is predicted for this CH··O hydrogen bond motif when harmonic vibrational zero-point energy contributions at the MP2/aug-cc-pVQZ level are incorporated. The two assigned large-amplitude donor OH librational modes of the 1:1 C_2H_4–H_2O complex observed at 255.0 and 187.5 cm^{-1}, respectively, confirm an intermolecular OH··π hydrogen-bonded conformatin having the H_2O subunit as the hydrogen bond donor to the π-cloud of C_2H_4. These two intermolecular vibrational modes alone constitute approximately 2/3 of the total change of vibrational zero-point energy associated with the weak π-cloud hydrogen bond formation. A reliable (semi)-empirical value for the change of vibrational zero-point energy of 4.0–4.1 $kJ \cdot mol^{-1}$ is proposed and the combination with quantum chemical calculations at the CCSD(T)-F12b/aug-cc-pVQZ level provides an estimate of 7.1±0.3 $kJ \cdot mol^{-1}$ for the dissociation energy D_0 of the C_2H_4–H_2O complex. In addition, tentative assignments for two strongly infrared active OH librational modes of the ternary 2:1 $H_2O(C_2H_4)_2$ complex having H_2O as a doubly OH··π hydrogen bond donor are proposed at 213.6 and 222.3 cm^{-1}. The

present work demonstrates that the intermolecular CH··O and OH··π hydrogen bond strengths are not determined solely by differences of electronic energy but to a significant degree by differences in vibrational zero-point energy contributions from large-amplitude intermolecular modes.

Supplemental Material

The electronic energies calculated at the MP2/aug-cc-pVQZ, CCSD(T)/aug-cc-pVQZ and CCSD(T)-F12/aug-cc-pVQZ level based on geometry optimizations at the counterpoise-corrected MP2/aug-cc-pVQZ level with harmonic vibrational zero-point energy corrections employing the MP2/aug-cc-pVTZ level are given as supplemental material together with the harmonic band origins for isotopic variants of the C_2H_2–H_2O and C_2H_4–H_2O complexes.

Acknowledgements

The authors appreciate interesting discussions with A. Engdahl. The authors acknowledge DTU Computing Center for access to the High Performance Computing services. RWL acknowledges financial support from the Danish Council for Independent Research's Sapere Aude Programme (Grant Ref.: 12-125248).

References

[1] Steiner, T. *Angewandte Chemie International Edition* **2002**, *41*(1), 48–76.

[2] Heger, M.; Andersen, J.; Suhm, M. A.; Wugt Larsen, R. *Phys. Chem. Chem. Phys* **2016**, *18*, 3739–3745.

[3] Iogansen, A. *Spectrochimica Acta Part A: Molecular and Biomolecular Spectroscopy* **1999**, *55*(78), 1585 – 1612.

[4] Peterson, K. I.; Klemperer, W. *The Journal of Chemical Physics* **1986**, *85*(2), 725–732.

[5] Andrews, A. M.; Kuczkowski, R. L. *The Journal of Chemical Physics* **1993**, *98*(2), 791–795.

[6] Engdahl, A.; Nelander, B. *Chemical Physics Letters* **1985**, *113*(1), 49–55.

[7] Engdahl, A.; Nelander, B. *The Journal of Physical Chemistry* **1986**, *90*(21), 4982–4987.

[8] Peterson, K. I.; Klemperer, W. *The Journal of Chemical Physics* **1984**, *81*(9), 3842–3845.

[9] Engdahl, A.; Nelander, B. *Chemical Physics Letters* **1983**, *100*(2), 129–132.

[10] Block, P. A.; Marshall, M. D.; Pedersen, L. G.; Miller, R. E. *The Journal of Chemical Physics* **1992**, *96*(10), 7321–7332.

[11] Rezaei, M.; Moazzen-Ahmadi, N.; McKellar, A. *Journal of Molecular Spectroscopy* **2012**, *272*(1), 19 – 22.

[12] Wugt Larsen, R.; Suhm, M. A. *The Journal of Chemical Physics* **2006**, *125*(15), 154314–154314.

[13] Wugt Larsen, R.; Suhm, M. *Physical Chemistry Chemical Physics* **2010**, *12*(29), 8152–8157.

[14] Kollipost, F.; Andersen, J.; Mahler, D.; Heimdal, J.; Heger, M.; Suhm, M. A.; Wugt Larsen, R. *Journal of Chemical Physics* **2014**.

[15] Kollipost, F.; Wugt Larsen, R.; Domanskaya, A. V.; Nörenberg, M.; Suhm, M. A. *The Journal of Chemical Physics* **2012**, *136*(15).

[16] Ceponkus, J.; Uvdal, P.; Nelander, B. *The Journal of Chemical Physics* **2008**, *129*(19), 194306.

[17] Andersen, J.; Heimdal, J.; Larsen, R. W. *Phys. Chem. Chem. Phys* **2015**, *17*(37), 23761–23769.

[18] Andersen, J.; Heimdal, J.; Wugt Larsen, R. *The Journal of Chemical Physics* **2015**, *143*(22).

[19] Andersen, J.; Heimdal, J.; Mahler, D. W.; Nelander, B.; Larsen, R. W. *The Journal of Chemical Physics* **2014**, *140*(9), 091103.

[20] Ceponkus, J.; Engdahl, A.; Uvdal, P.; Nelander, B. *Chemical Physics Letters* **2013**, *581*, 1–9.

[21] Ceponkus, J.; Nelander, B. *The Journal of Physical Chemistry A* **2004**, *108*(31), 6499–6502.

[22] Ceponkus, J.; Uvdal, P.; Nelander, B. *The Journal of Chemical Physics* **2010**, *133*(7), 074301.

[23] Ceponkus, J.; Uvdal, P.; Nelander, B. *The Journal of Physical Chemistry A* **2010**, *114*(25), 6829–6831.

[24] Moazzen-Ahmadi, N.; McKellar, A. *International Reviews in Physical Chemistry* **2013**, *32*(4), 611–650.

[25] Bouteiller, Y.; Tremblay, B.; Perchard, J. *Chemical Physics* **2011**, *386*(13), 29 – 40.

[26] Ceponkus, J.; Karlström, G.; Nelander, B. *The Journal of Physical Chemistry A* **2005**, *109*(35), 7859–7864.

[27] Kalugina, Y. N.; Cherepanov, V. N.; Buldakov, M. A.; Zvereva-Lote, N.; Boudon, V. *Journal of Computational Chemistry* **2012**, *33*(3), 319–330.

[28] Benedict, W.; Gailar, N.; Plyler, E. K. *The Journal of Chemical Physics* **1956**, *24*(6), 1139.

[29] Gaussian09 Revision D.01. Frisch, M. J.; Trucks, G. W.; Schlegel, H. B.; Scuseria, G. E.; Robb, M. A.; Cheeseman, J. R.; Scalmani, G.; Barone, V.; Mennucci, B.; Petersson, G. A.; Nakatsuji, H.; Caricato, M.; Li, X.; Hratchian, H. P.; Izmaylov, A. F.; Bloino, J.; Zheng, G.; Sonnenberg, J. L.; Hada, M.; Ehara, M.; Toyota, K.; Fukuda, R.; Hasegawa, J.; Ishida, M.; Nakajima, T.; Honda, Y.; Kitao, O.; Nakai, H.; Vreven, T.; Montgomery, Jr., J. A.; Peralta, J. E.; Ogliaro, F.; Bearpark, M.; Heyd, J. J.; Brothers, E.; Kudin, K. N.; Staroverov, V. N.; Kobayashi, R.; Normand, J.; Raghavachari, K.; Rendell, A.; Burant, J. C.; Iyengar, S. S.; Tomasi, J.; Cossi, M.; Rega, N.; Millam, J. M.; Klene, M.; Knox, J. E.; Cross, J. B.; Bakken, V.; Adamo, C.; Jaramillo, J.; Gomperts, R.; Stratmann, R. E.; Yazyev, O.; Austin, A. J.; Cammi, R.; Pomelli, C.; Ochterski, J. W.; Martin, R. L.; Morokuma, K.; Zakrzewski, V. G.; Voth, G. A.; Salvador, P.; Dannenberg, J. J.; Dapprich, S.; Daniels, A. D.; Farkas, .; Foresman, J. B.; Ortiz, J. V.; Cioslowski, J.; Fox, D. J. **2009**.

[30] Werner, H.-J.; Knowles, P. J.; Knizia, G.; Manby, F. R.; Schtz, M. *WIREs Comput. Mol. Sc.* **2012**, *2*, 242–253.

[31] Molpro, version 2015.1, a package of ab initio programs. Werner, H.-J.; Knowles, P. J.; Knizia, G.; Manby, F. R.; Schütz, M.; Celani, P.; Györffy, W.; Kats, D.; Korona, T.; Lindh, R.; Mitrushenkov, A.; Rauhut, G.; Shamasundar, K. R.; Adler, T. B.; Amos,

R. D.; Bernhardsson, A.; Berning, A.; Cooper, D. L.; Deegan, M. J. O.; Dobbyn, A. J.; Eckert, F.; Goll, E.; Hampel, C.; Hesselmann, A.; Hetzer, G.; Hrenar, T.; Jansen, G.; Köppl, C.; Liu, Y.; Lloyd, A. W.; Mata, R. A.; May, A. J.; McNicholas, S. J.; Meyer, W.; Mura, M. E.; Nicklass, A.; O'Neill, D. P.; Palmieri, P.; Peng, D.; Pflüger, K.; Pitzer, R.; Reiher, M.; Shiozaki, T.; Stoll, H.; Stone, A. J.; Tarroni, R.; Thorsteinsson, T.; Wang, M. **2015**.

[32] Møller, C.; Plesset, M. S. *Physical Review* **1934**, *46*, 618–622.

[33] Krishnan, R.; Pople, J. A. *International Journal of Quantum Chemistry* **1978**, *14*(1), 91–100.

[34] Kendall, R. A.; Dunning, Jr., T. H.; Harrison, R. J. *The Journal of Chemical Physics* **1992**, *96*(9), 6796–6806.

[35] Pople, J. A.; Head-Gordon, M.; Raghavachari, K. *The Journal of Chemical Physics* **1987**, *87*(10), 5968–5975.

[36] Adler, T. B.; Werner, H.-J. *The Journal of Chemical Physics* **2011**, *135*(14), 144117.

[37] Ransil, B. J. *The Journal of Chemical Physics* **1961**, *34*(6), 2109–2118.

[38] Boys, S.; Bernardi, F. *Molecular Physics* **1970**, *19*(4), 553–566.

[39] Tzeli, D.; Mavridis, A.; Xantheas, S. S. *The Journal of Chemical Physics* **2000**, *112*(14), 6178–6189.

[40] Frisch, M. J.; Pople, J. A.; Del Bene, J. E. *The Journal of Chemical Physics* **1983**, *78*(6), 4063–4065.

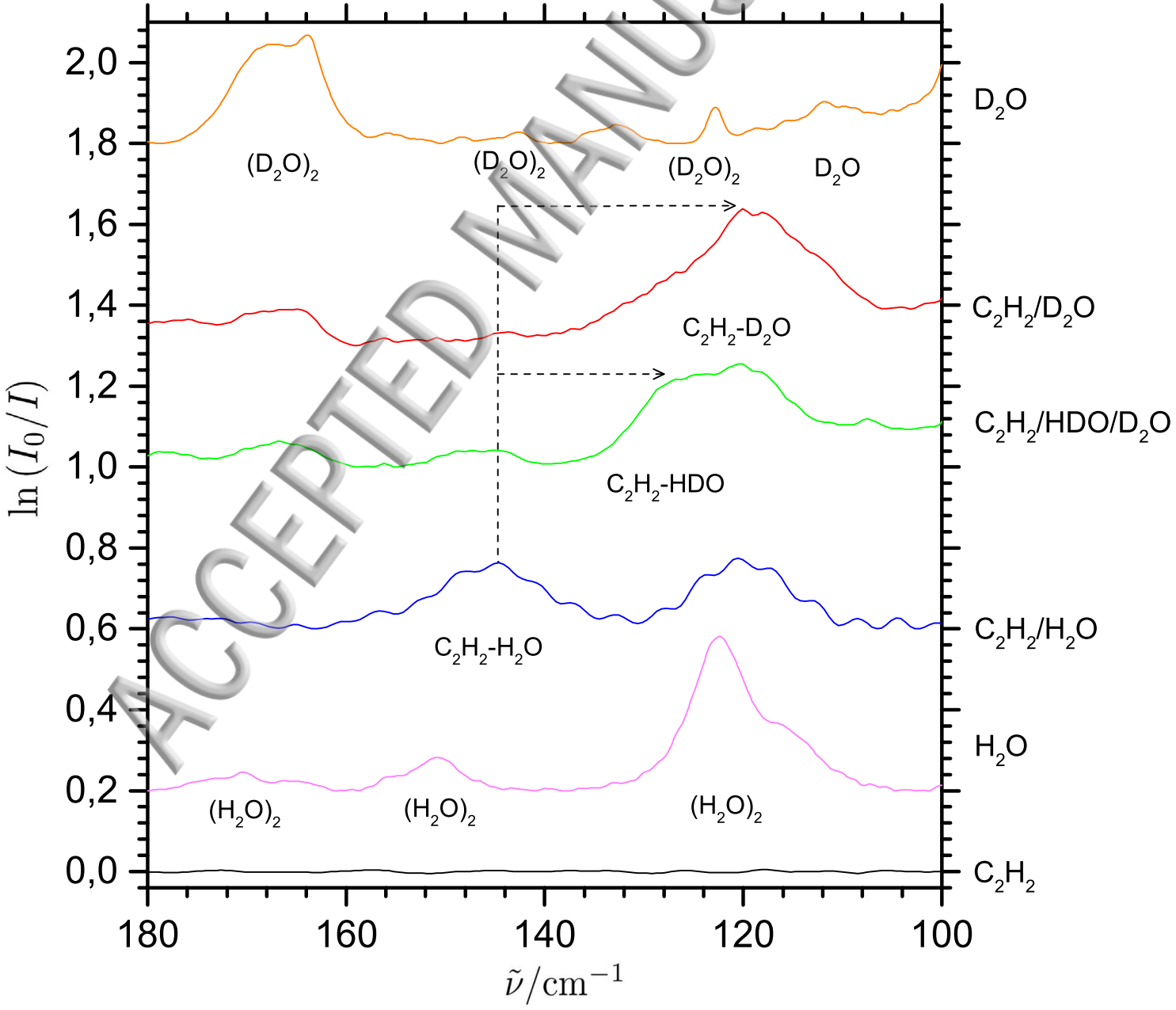

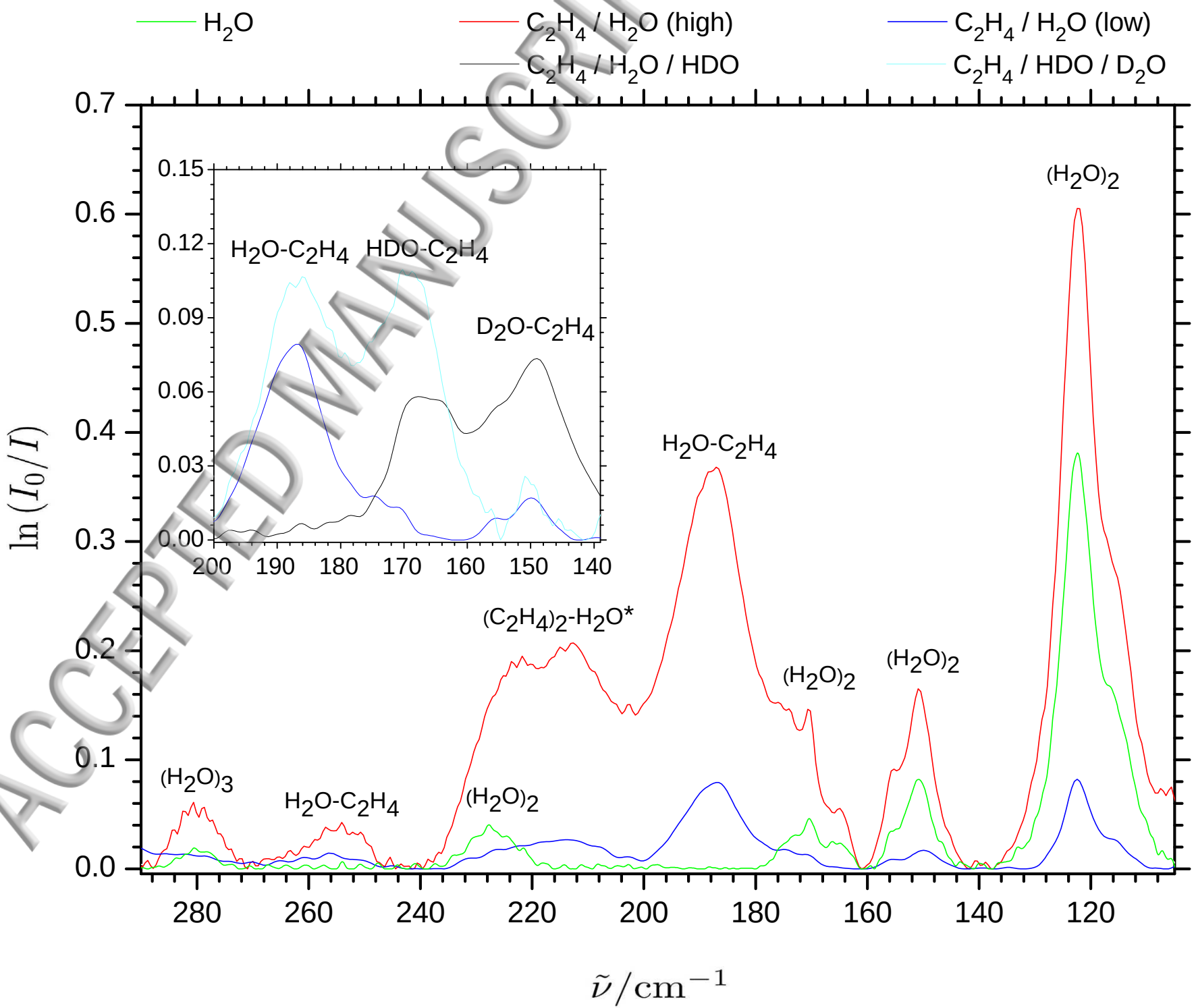

$\tilde{\nu}/\mathrm{cm}^{-1}$